Theor. Comput. Fluid Dyn. (2013) 27:273–295
DOI 10.1007/s00162-012-0267-9

ORIGINAL ARTICLE

D. O. Lignell · A. R. Kerstein · G. Sun · E. I. Monson

Mesh adaption for efficient multiscale implementation of one-dimensional turbulence

Received: 31 July 2011 / Revised: 2 March 2012 / Accepted: 6 April 2012 / Published online: 29 April 2012

Abstract One-Dimensional Turbulence (ODT) is a stochastic model for turbulent flow simulation. In an atmospheric context, it is analogous to single-column modeling (SCM) in that it lives on a 1D spatial domain, but different in that it time advances individual flow realizations rather than ensemble-averaged quantities. The lack of averaging enables a physically sound multiscale treatment, which is useful for resolving sporadic localized phenomena, as seen in stably stratified regimes, and sharp interfaces, as observed where a convective layer encounters a stable overlying zone. In such flows, the relevant scale range is so large that it is beneficial to enhance model performance by introducing an adaptive mesh. An adaptive-mesh algorithm that provides the desired performance characteristics is described and demonstrated, and its implications for the ODT advancement scheme are explained.

Keywords Turbulence · Numerical simulation · Mesh adaption · Multiscale methods

1 Introduction

The most challenging multiscale problems are those in which cross-scale couplings are prevalent over a wide range of length and time scales, requiring modeling approaches that resolve the relevant scales efficiently. Turbulent atmospheric flows, such as in boundary layers and clouds, present such challenges. To address these and related cases, a turbulence simulation method termed One-Dimensional Turbulence (ODT) has been developed [10]. For affordable application to a wide scale range, ODT is formulated in one spatial dimension (1D). For typical atmospheric flow applications, it is applied to a vertical column [14], as in single-column modeling (SCM) [7].

Communicated by R. Klein.

D. O. Lignell (✉) · G. Sun · E. I. Monson
Department of Chemical Engineering, Brigham Young University, Provo, UT 84602, USA
E-mail: davidlignell@byu.edu
Tel.: +801-422-1772
Fax: +801-422-0151

G. Sun · E. I. Monson
Tel.: +801-422-6243
Fax: +801-422-0151

A. R. Kerstein
Combustion Research Facility, Sandia National Laboratories, Livermore, CA 94551-0969, USA
E-mail: alan.kerstein@gmail.com
Tel.: +925-820-5063
Fax: +925-820-5063

In a different context [23], an adaptive-mesh formulation of ODT was introduced in order to improve the numerical accuracy of a spatial-marching scheme (involving no time advancement) for ODT. This formulation has since been improved and used in an application involving temporal advancement [6], and a spatial-marching application is in progress. Initial spatial-marching results are presented in Sect. 6. Here, the improved adaptive-mesh formulation is described, preceded by an overview of the ODT modeling approach.

2 Overview of ODT

ODT is described here in enough detail to prepare for discussion of the adaptive-mesh formulation. Additional information is available elsewhere [10,11].

The ODT spatial coordinate is denoted x, which can be vertical or horizontal depending on the application. One or more velocity components, and scalar properties pertinent to the application (including density or a density surrogate for all variable-density applications) are advanced, temporally or spatially, on this domain. For the baseline illustrative case considered here, the dependent variables are three velocity components (u, v, w), density ρ, and a conserved scalar θ. Variants of this case are also considered.

Temporal advancement is applied to an ODT domain that is deemed to be fixed in space, as in the temporal case mentioned in Sect. 1. Spatial advancement is applied to a domain that is deemed to march in a direction normal to the domain. For example, if the domain direction x is horizontal, then ODT can generate a rendering of a 2D cut through the flow by marching in the vertical direction, as in an application of spatial advancement to planar vertical jets and plumes [23]. Mathematical statements of these and related ODT formulations are presented in [5].

Evolution of property profiles on a time-advancing ODT domain can be interpreted as representing evolution along a line of sight through 3D turbulence. However, ODT advancement differs from the latter, notably because ODT is subject only to domain-aligned property fluxes while the line of sight is subject to fluxes in all directions. This is reasonable in an average sense provided that the flow of interest is homogeneous in directions normal to the line of sight. On an instantaneous basis, though, this requires a mechanism for ODT to generate property fluctuations that usually depend on the occurrence of folding and straining motions in 3D turbulence.

For this purpose, the advective term in the advancement equations (see Sect. 5.1) is replaced by a randomly generated sequence of instantaneous maps, each of which is applied to some chosen interval $[x_0, x_0 + l]$ of the ODT domain and can be viewed heuristically as the model analog of a turbulent eddy occurring at the time of the map and within the chosen interval. The map, denoted the 'triplet map,' compresses the chosen interval to one third of its original size and fills the original interval with three such compressed copies, with the middle one spatially inverted. This map is measure preserving (the 1D analog of the solenoidal flow) and does not introduce discontinuities into property profiles.

To model the interaction of pressure fluctuations and advection, an 'eddy event' is subject to an additional operation after the triplet map is applied. Namely, functions J and K, each with fixed shape but eddy-dependent support $[x_0, x_0 + l]$, are used to modify the mapped velocity profiles additively as follows: $s \rightarrow s + b_s J + c_s K$, where s is u, v, or w, and coefficients b_s and c_s are chosen to conserve momentum and total energy. (Mathematically, J and K are wavelets. They have units of length so the coefficients have units of inverse time. The functional forms that are used are discussed in the "Appendix".) Thus, the six coefficients $(b, c)_{u,v,w}$ are subject to four constraints. The other two needed constraints are obtained by requiring equalization of the 'available kinetic energies' (defined in the "Appendix") of the three velocity components within the map interval. This reflects the phenomenological notion that turbulence tends toward an isotropic state because repeated changes of fluid-parcel orientation mediated by pressure fluctuations wash out any direction-dependent tendencies.

Flow advancement in ODT consists of advancement of a 1D specialization of the 3D governing equations, omitting advective and pressure terms (but possibly including an imposed mean pressure gradient), punctuated by instantaneous randomly occurring eddy events. Apart from the structural features of ODT that have been described, the physical content of the model that primarily determines its predictive capability is the procedure for sampling the sequence of eddy-event times and spatial intervals. The procedure, outlined in the "Appendix", involves a determination of the relative likelihoods of possible eddy events analogous to the determination of fluxes between cell pairs in the transilient model [28]. In another sense, it is analogous to the concept of convectively available potential energy (CAPE) [28]. Namely, the collection of adiabatic displacements induced by a triplet map results in a gravitational potential energy change in a buoyant stratified flow that can be scaled using the eddy size l and a reference density (assuming Boussinesq flow) to obtain a rate (inverse time scale). (Shear effects are included, though neglected in this example for simplicity.) The rates of all possible eddies can be normalized to obtain an ‘eddy rate distribution’ that can in principle be sampled to generate the random sequence of eddy events. Because this distribution changes whenever the flow state changes, literal implementation of this approach would be very costly, so a mathematically equivalent but more efficient sampling procedure is used, as explained in the “Appendix” and in [11].

The CAPE analogy used above to motivate eddy rate determination for buoyant stratified flow is based on a vertically oriented ODT domain. Some buoyant stratified flows are more readily represented using a horizontal ODT domain. For example, consider a planar plume modeled in ODT by starting from a motionless state with a tent-shaped initial buoyancy profile. In the Boussinesq approximation, upward flow develops due to buoyancy higher than the far-field reference value. This mechanism is represented by introducing a gravitational forcing term in the 1D momentum equation. This term induces horizontal variation of vertical velocity, hence shear, which in this case is the only contribution to the eddy rate because horizontal maps do not change the gravitational potential energy. Both temporally developing (vertically invariant) and spatially developing plumes can be simulated (see Sect. 5). This example illustrates that given physics, in this case buoyancy effects, can be represented in different ways in ODT (e.g., in the 1D governing equations or in the physical modeling of the eddy rate) depending on the model set-up (e.g., horizontally vs. vertically oriented computational domain).

The procedure for enforcement of the applicable conservation laws highlights some features of the ODT representation of various flow configurations. By construction, the triplet map preserves the domain integrals of all fluid state variables, so in particular, it conserves momentum and kinetic energy. However, body forces can change momentum and kinetic energy, as in the case of buoyancy effects in a vertically oriented ODT simulation. In this case, conservation of total energy implies that the gravitational potential energy change induced by a triplet map requires an equal-and-opposite kinetic energy change. The functions J and K mentioned above enforce this change, and thus play an essential role in the implementation of conservation laws as well as in the representation of the tendency toward isotropy.

If a map induces an increase in gravitational potential energy (corresponding to negative CAPE, i.e., stable stratification), then the functions J and K enforce a corresponding reduction of kinetic energy in the map interval. The dependence of the kinetic energy change on the coefficients b_s and c_s is such that any amount of kinetic energy can be added, but the amount that can be removed is bounded, reflecting the finite amount of kinetic energy that is available. As a result, conservation of total energy cannot be enforced if the stratification in the map interval is sufficiently stable, in which case the map is deemed to be energetically forbidden. This is the model analog of turbulence suppression above a critical Richardson number Ri_c. In particular, the eddy rate distribution is formulated so that the model value of Ri_c is the same as the value $Ri_c = \frac{1}{4}$ known from linear stability theory [14].

Dimensionally, it is straightforward to associate the CAPE in a map interval with an eddy rate (inverse time scale) using the interval size and a reference density, and hence to formulate an eddy rate distribution representing buoyant forcing. Shear forcing does not involve conversion of energy from one form to another, so its contribution to the eddy rate need not be based on energetic considerations, but doing so leads to a consistent framework for treating mixed convection as well as pure shear forcing. See the “Appendix” and cited references for details.

The model description thus far is general enough to encompass the two main applications to date, combustion and buoyant stratified flows, as well as various canonical cases that have been simulated. Case-specific features appear in the 1D-specialized governing equations, in the physical modeling of the dependence of the eddy rate on the flow state, and in the initial and boundary conditions.

In what follows, the adaptive-mesh ODT formulation is described initially from a general perspective, but then with an emphasis on combustion because this application requires the most detailed consideration to date of physical modeling within the adaptive-mesh formulation. There are no features of adaptive-mesh implementation that are specific to the aforementioned methods of incorporation of buoyancy effects, so there is no further explicit consideration of buoyant stratified flow. The first published description of mesh adaption for ODT [23] is for a spatially developing fire plume application involving both buoyancy and combustion.

3 Discretization and map implementation

The computational domain corresponds to an x range denoted $[0, L]$, consisting of n cells with face locations x_i, where $x_1 = 0$ and $x_{n+1} = L$. All property profiles are constant in each cell. For eddy-event implementation, this is the only discrete approximation. The mathematical definition of the triplet map stated in Sect. 2

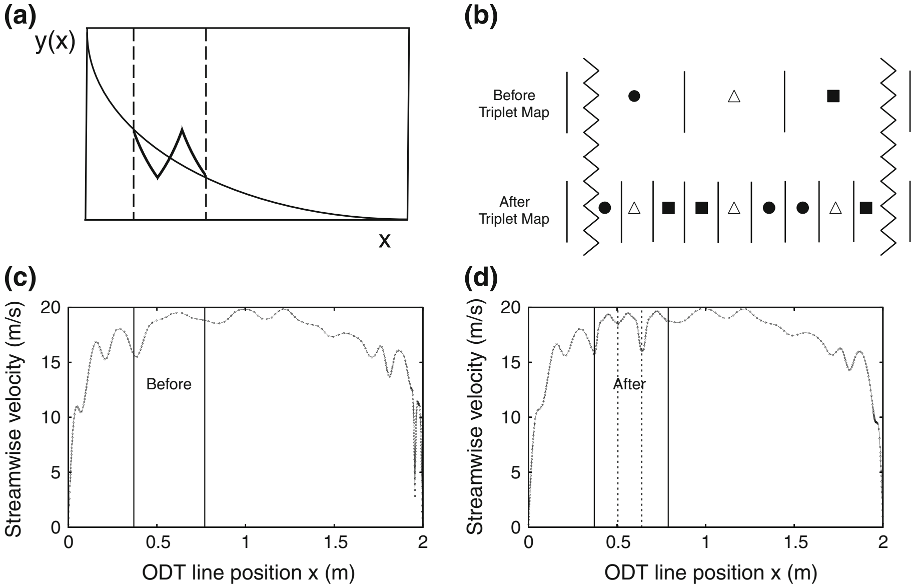

Fig. 1 Illustration of the triplet map for stochastic eddy events modeling advection in ODT. Plot **a** shows a profile $y(x)$ before (*thin line*) and after (*thick line*) a triplet map occurring between the two *dashed vertical lines*. Plot **b** illustrates the placement and size of grid cells during a triplet map, where the *vertical saw-tooth lines* denote the map edges. In **c** and **d**, cell centers are connected by *curves*, *solid vertical lines* bound the mapped region, and in **d**, *dashed vertical lines* separate the compressed copies (center copy spatially *inverted*) of the original property profile within the mapped region

can be applied without further approximation by displacing face locations to compress the map interval as prescribed, then creating new face locations corresponding to the additional copies, and finally, displacing the face locations in the middle copy to invert that copy. (In practice, these steps can be combined.)

Figure 1 illustrates the map procedure. Plot (a) is a schematic showing how an original profile in an eddy region is replaced with three copies, each compressed spatially by a factor or three, with the middle copy inverted spatially. Plot (b) shows how this is done with respect to grid cells where each cell is directly compressed and the number of cells triples. If an eddy is accepted, the original cell is split at the eddy location. The assumed piecewise-constant profile (constant in each cell) is utilized in implementing the map. Plots (c) and (d) show the mapping process in a channel flow simulation (discussed in Sect. 5.1.1).

The discrete statement of non-creation of discontinuities is that faces in their new locations and ordering but with the original indexing (now with repetition of some indices) are consecutive with respect to index values, though no longer monotonic. Properties in each of the new cells have the same values as in the original cell bracketed by face variables with the same pair of indices (possibly in reverse order). This fully prescribes triplet-map implementation on the adaptive mesh.

In contrast, the triplet map on a fixed uniform mesh is implemented as a permutation of $3m$ cells, where m is an integer. For a map of fixed physical size, m increases with increasing mesh refinement, with mathematically exact implementation of the triplet map only in the large-m limit. A physically important property of the triplet map is its mean-square displacement within the mapped interval, which determines its contribution to the eddy diffusivity corresponding to a given map sequence. A discrete map of fixed physical size induces a mean-square displacement that is an increasing function of m. For $m = 2$, it is half the value in the mathematically exact large-m limit, showing that the effect is significant. This numerical error is corrected by introducing an m-dependent adjustment of the sampling rates. Similarly, the limitation to a discrete set of map locations and sizes for the uniform mesh requires spatial discretization of the eddy rate distribution. Such manipulations are not needed in the adaptive-mesh implementation.

4 Mesh adaption

Mesh adaption is needed for the two key processes occurring in ODT: (1) application of triplet maps that model advective processes; and (2) diffusive (and possibly reactive) advancement of property fields. The adaptive-mesh implementation of the triplet map triples the number of grid points in the map (eddy) region, consistent with the associated increase of property gradients and tripling of local extrema. The resulting mesh is not necessarily well suited for discretization of property profiles. For example, small cells may be introduced at the boundaries of a map region, see Fig. 1, which would impose stringent time-step constraints. Also, adjacent cells (at boundaries) may be created with an overly large size ratio. Hence, adaption of the triplet mapped region is appropriate.

Property fluctuations in ODT reflect a balance between the wrinkling effect of eddy events (which occur instantaneously) and the smoothing effect of the intervening diffusive advancement. This advancement smooths property gradients, annihilating local extrema, and results in fields that may be over-resolved at the end of the diffusive advancement, which is typically performed with a fixed number of grid points. Because of this smoothing, mesh adaption is needed in the eddy region following diffusive advancement.

In regions where eddy events are relatively infrequent, diffusion can proceed without interruption by an eddy for a long enough time so that property profiles undergo significant additional smoothing and further coarsening of the mesh is warranted. To identify such regions on the fly, a fixed, uniform grid of timing zones is introduced along the spatial domain, each of which tracks the elapsed time since it was last intersected by an eddy event. Based on a criterion that compares the largest such elapsed time to a multiple of the diffusive CFL time, regions unaffected by eddy events for a relatively long time are subject to mesh adaption.

Mesh adaption is applied in this selective manner because it induces numerical transport. Applying mesh adaption only when and where it is most needed minimizes any resulting numerical transport. (Section 6 further discusses numerical dissipation due to mesh adaption for the channel flow case mentioned.) The adaption strategy is thus specialized with regard to the unique features of ODT advancement. Although its implementation in one spatial dimension avoids the complications specific to multi-dimensional mesh management, it is seen that some degree of care and specialization is nevertheless beneficial.

While diffusive advancement tends to smooth scalar profiles, in flows with scalar source terms (such as buoyant or reactive flows), diffusive advancement can result in increases in property gradients, both in the eddy region and elsewhere. Additionally, the Lagrangian formulation discussed below in Sect. 5 may result in expanding or contracting cell sizes. In these cases, it may be necessary to adapt a greater portion of the line after (or even during) the diffusion step.

To summarize, mesh adaption occurs in the eddy region after triplet map events, in the eddy region (or beyond) after diffusive advancement, and in regions that have not been adapted for sufficient time. A series of four plots showing the mesh-adaption behavior after an eddy, eddy adaption, diffusion, and adaption after diffusion is shown in Fig. 2.

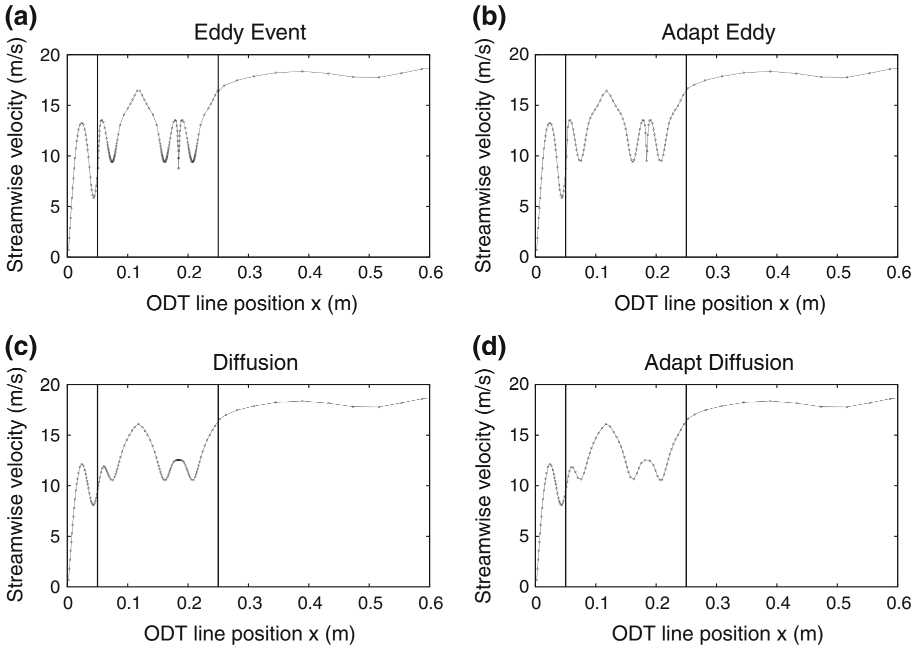

Fig. 2 ODT mesh in an eddy region (bounded by *solid vertical lines*) at four sequential stages

4.1 Mesh-adaption procedure

The ODT grid is formulated with 1D control volumes (cells), each bounded by two cell faces, with the cell center midway between the faces. All mesh adaption is performed by merging and splitting cells. Property profiles are assumed uniform within cells for this process, and the merging and splitting are done conserving mass, momentum, etc. (for temporal ODT cf. Sect. 5.1), or the corresponding flux (for the spatial formulation cf. Sect. 5.2). Cell merging does not conserve higher moments of properties, notably energy. The selective application of mesh adaption is intended to mitigate such artifacts.

Adaption of the mesh in a designated size-L region of the domain is based on adequate adaption of one or more property profiles (the primary adaption, discussed below) and subject to the following three constraints:

1. Cells should be smaller than a given maximum size (which is almost never an issue).
2. Cells should be larger than a pre-specified minimum size (larger than a specified fraction of the domain).
3. A cell should not be larger or smaller than its two neighbors by more than a factor of 2.5 (termed the *2.5 rule*).

The last constraint prevents mesh irregularities that would degrade the accuracy of the diffusive advancement. The factor 2.5 is not crucial, other factors will work. Central difference errors were found to be approximately linear in this factor over the range one to four. A smaller factor (approaching unity) will be more accurate, but require more grid points, while a larger factor incurs larger error but reduces the number of grid points. The factor 2.5 is a reasonable value and any unacceptable discretization errors may be mitigated by reducing the overall grid spacing (increasing the total number of grid points). The first two constraints rarely need to be enforced. They are backstops to handle atypical conditions that are not adequately managed by the main adaption procedure. The minimum and maximum cell sizes are user-specified inputs that must be determined a-priori, normally based on computational resource limitations, experience, test simulations, or based on the smallest expected property length scales (e.g., a factor of the Kolmogorov length scale). Each of these conditions relates only to the grid cell locations themselves and are not based on the structure of the property profiles. The primary adaption procedure is intended to provide adequate but not excessive spatial resolution of its features. Adaption may be based on multiple profiles, but adaption based on one profile (such as the streamwise velocity) is discussed first, then generalized to several profiles.

There are many ways to adapt a given profile. One is to adapt based on local gradients and curvatures in the profile subject to the above constraints. For instance, one may split any large cells, then merge any small cells, then merge cells in regions of small gradients and curvatures, and split cells in regions of large gradients, and finally impose the 2.5 rule. This was implemented, but is somewhat cumbersome as one process should not invalidate a previous one, so attention must be paid to order of operation within the grid. Also, introducing cell bias based on direction of processing must be avoided.

An alternative approach is implemented that is based on distributing cells in the domain so that the arc length of the adapted property profile is nominally the same between pairs of cells. Conceptually, consider a string laid along a graph of y versus x, then stretched out. New cells are marked uniformly along the string, which is then refitted to the $y(x)$ graph. The x locations of the marked string define the new grid. These new x locations X are then processed according to the grid quality constraints above. Once X is determined, the ODT grid cells are split to form cell faces that are present in X, but not in the original ODT grid. Then, ODT cells are merged to eliminate cell faces present in the original ODT grid that are not in X. The resulting ODT grid matches X and may have a different number of grid points than before adaption. This procedure is simple to implement and naturally places more cells in high-gradient regions and fewer cells in low-gradient regions, as desired. Figure 3 illustrates the meshing procedure: the arc distance function is computed for each cell, then summed to obtain the cumulative arc length, which is then uniformly divided and interpolated to the new x-grid, and then used to obtain the new ODT line grid and profiles.

The key parameter governing the mesh adaption is the number density of grid points, N_{dens}, or the number of points per unit arc length. This parameter allows the total number of cells to adjust to the level of variation in the profile. Because x and y have different units, they are centered and scaled to vary on $[0,\ 1]$. More precisely, when adapting a given subregion L, the adaption is based on x and y in L, but the scaling is based on the minimum and maximum extents over the whole domain so that the grid density parameter is consistent on any subregion. Hence, the mesh in a given region L is similar whether region L is adapted alone, or the whole domain is adapted.

The arc length Δs_i for a given cell is computed based on a piecewise-linear representation,

$$\Delta s_i = \sqrt{\Delta x_i^{*2} + \Delta y_i^{*2}}, \tag{1}$$

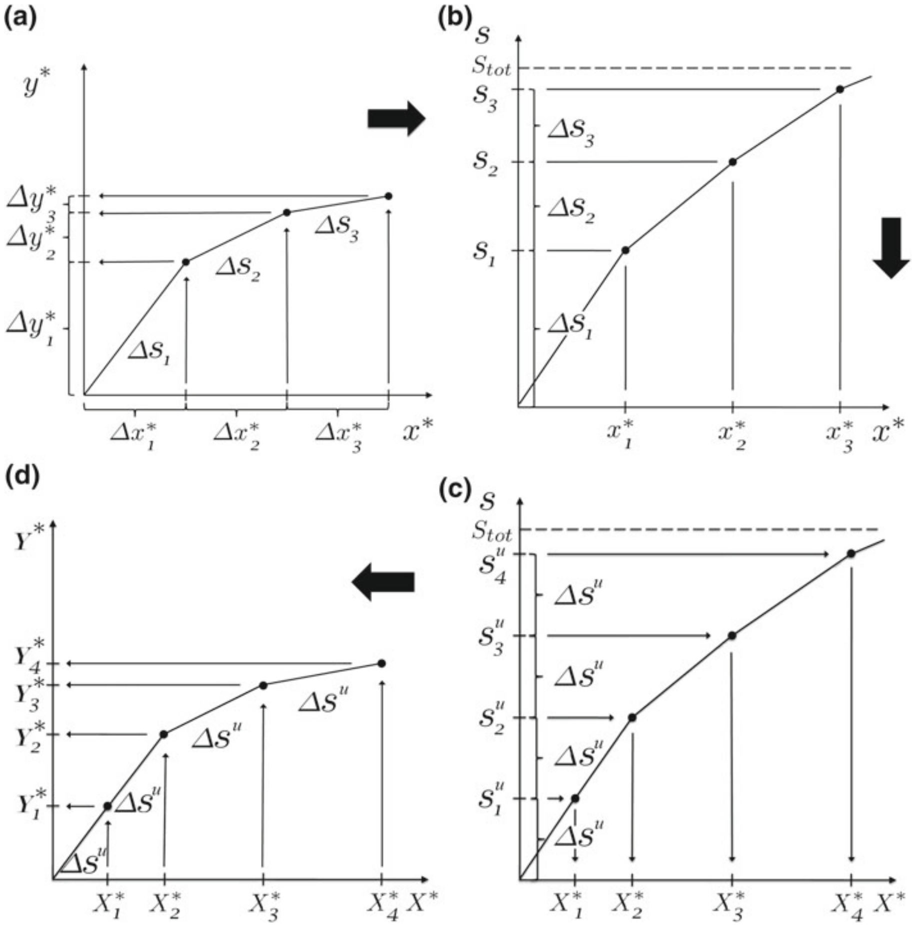

Fig. 3 Illustration of the mesh-adaption procedure (proceed *clockwise*)

where stars denote the scaled quantity, Δx_i^* is the cell size, and Δy_i^* is evaluated at cell faces (linearly interpolated from cell centers). The total arc length S_{tot} is just the sum of the individual Δs_i for the cells. Given S_{tot}, a uniform arc length grid s_i^u is given by $\Delta s_i^u = S_{\text{tot}}/\text{int}(N_{\text{dens}} S_{\text{tot}})$, where int() denotes the integer part. The new grid X_i^* is computed by interpolating x_i^* and s_i, to X_i^* and s_i^u. This grid X_i^* is then un-scaled to X_i.

Often, it is desired to adapt the grid such that multiple property profiles are adequately resolved. This is especially important if the variations in the profiles are not spatially collocated. Therefore, any number of properties can be chosen for inclusion in the adaption procedure. Then when computing Δs_i for given i, the largest of the Δy_i^{*2} values for the included properties is used. This results in over-resolution of some of the profiles, but is necessary if the profiles reside on the same grid. (Incidentally, multiple grids have been used in adaptive-mesh ODT for combustion applications, with momentum on one grid and combustion scalars on another.) An alternative approach is to adapt each profile independently to obtain a series of X grids (one for each profile), then take the union of these. This approach can result in redundant resolution, however, such as two points that nearly overlap when one point would be sufficient for both profiles.

Given the primary adaption procedure, one could easily modify the approach. For instance, regions with no fluctuations (gradients) tend to have more grid cells than are necessary since those regions have arc length from the Δx_i^* component. This is not usually of significant consequence because the majority of the grid is in regions of high fluctuations. However, one can weight the arc length function s_i based on local gradients (for instance, through a multiplier of Δy_i^*), or local curvatures, etc. This is essentially what is done when adapting multiple properties and choosing the largest of the Δy_i^* among the adapted properties.

Once the primary adaption procedure is performed, the grid is processed to eliminate cells that are smaller than a specified fraction of the domain length. This is done by marking all small cells and sorting in order of increasing size. Beginning at the smallest, a cell is merged with the smaller of its two neighbors until the cell is above the size threshold. A small cell may be merged with another small cell, in which case that other small cell is eliminated from the list. This procedure eliminates the small cells without directional bias.

The 2.5 rule is imposed so that adjacent cells are not too different in size. A list of cells that offend their right neighbor is created. Given an offending cell i and its right neighbor ip, the larger of the two cells is split one or more times as needed to satisfy the criterion. Suppose i is the larger cell. If one split is needed, then i is split in half. If two splits are needed, then i is split in half, then the half next to ip is split so that cell i is split into three parts with sizes $\frac{1}{2}$, $\frac{1}{4}$, $\frac{1}{4}$ the original. For three splits, we have sizes $\frac{1}{2}$, $\frac{1}{4}$, $\frac{1}{8}$, $\frac{1}{8}$ the original, etc. Splitting i may result in a new offense between i and its left neighbor, so these two cells must also be checked. In this manner, the domain is traversed until the criterion is satisfied, or the domain edge is reached. In order to traverse in one direction, however, cells must increase in that direction, and since that traverse implies geometric growth of cells, the algorithm does not travel too far. The routine is implemented recursively and yields a unique output independent of the starting point.

Cell property profiles are assumed uniform within cells. This simplifies conservative merging and splitting of cells. Merging introduces no complications. Splitting cells allows some flexibility of the resulting property values in cells. Split cell profiles are interpolated using a conservative parabolic profile subject to the constraint that no new extrema are generated. The parabola is defined such that it passes through the two neighbor cells, and that the integral of the property in the pre-split cell equals that of the parabola. Split cell property values (uniform in the cell) are then specified to match the integral of the parabola in the region of the split cell.

5 Diffusive advancement on the non-uniform mesh

The mesh-adaption strategy and adaptive implementation of triplet maps were discussed above. Here, the diffusive advancement of momentum and scalar fields is discussed. This implementation utilizes a Lagrangian formulation in which cells expand and contract such that no mass crosses cell boundaries. There are two formulations of ODT, (1) *temporal*, in which the 1D line evolves in time; and (2) *spatial*, in which the line evolves in a spatial direction orthogonal to the line in a nominally steady flow. For constant density, temporal advancement, there is no change to the mesh since in 1D there is no dilatation. For spatial advancement, or variable-density temporal advancement, the mesh evolves during diffusion.

The broadest benefit of the adaptive-mesh implementation is reduction of the number of mesh cells needed to span a given range of spatial scales. An additional benefit arises from the implicit treatment of 1D advection from dilatation that occurs in spatial flows or temporal flows with variable density. This dilatation is denoted by a velocity field $U(x)$, which is distinct from the ODT velocities u, v, and w that induce advection only indirectly through the specification of eddy events. An Eulerian implementation of this advection can reduce the advancement time step significantly because U is generally much larger than diffusion velocities, which otherwise control the time step. It is well known that Lagrangian advection can circumvent this time-step limitation; and this is straightforward to implement in 1D, as described below.

In this section, we describe in detail the temporal and spatial formulations of ODT and introduce two temporally evolving planar configurations for demonstration: the channel flow and the reacting jet. While the emphasis here is on planar ODT, the model has also been extended to cylindrical coordinates [15].

5.1 Temporal advancement

Temporal ODT evolves momentum and scalar fields on the ODT line in time. The temporal formulation is the original and most straightforward formulation of ODT, but is limited to 1D unsteady configurations. Suitable applications include those with a single direction of statistical inhomogeneity, such as the temporally evolving planar mixing layer, channel flow, and jet. The latter two are introduced to give concrete examples and to motivate the description of the evolution equations below. Results from these flows are discussed later.

5.1.1 Channel flow

The planar channel flow is a statistically stationary flow between two infinite parallel plates. The flow is driven by a pressure gradient, which is a source term for streamwise momentum. Transport equations are solved for three components of momentum, which define the flow, and whose dynamics determine the stochastic sequence of eddy events. Figure 4 shows the set-up of the channel flow in 1D with an instantaneous and mean

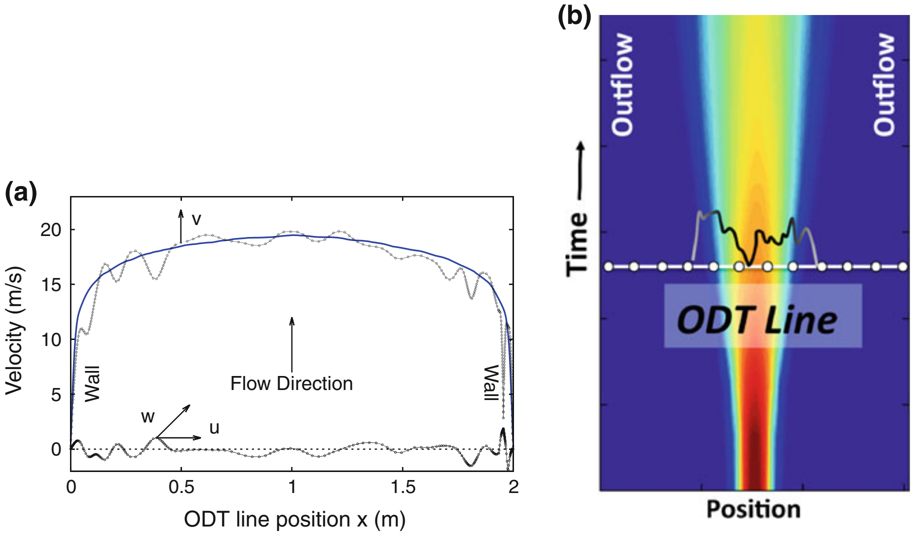

Fig. 4 Channel flow (**a**) and temporal jet (**b**) configurations. The channel flow shows typical instantaneous and mean velocity component profiles. The temporal jet shows mean mixture fraction contours with a typical instantaneous mixture fraction profile and ODT line position overlaid

wall-normal profile of the streamwise velocity. The instantaneous streamwise velocity v is shown, along with the mean velocity $\langle v \rangle$ after a long run time. Also shown are the instantaneous u and w components of velocity, here included in the ODT formulation although an ODT formulation involving only the streamwise component of velocity captures the salient flow features equally well. For this flow configuration, the u and w components in ODT are the same, reflecting the reduced representation of the flow in ODT. The ODT line is horizontal with the cell center locations indicated. The configuration requires an initial condition and boundary conditions for the velocities.

5.1.2 Temporal jet

The planar temporally evolving jet is similar in configuration to the channel flow, but rather than impose the no-slip boundary conditions on velocity, standard zero-gradient outflow conditions are imposed. The planar configuration implies a slot jet of given slot width with infinite spanwise expanse. The initial condition for the jet is usually a top-hat profile for the velocity field, with high velocity in the center, and lower velocity in the free stream. This flow is an idealization of real jets, which evolve spatially in 3D, but the jet is idealized as a boundary layer flow with gradients primarily in the cross-jet direction (the ODT line direction). Furthermore, the temporal jet assumes the flow is statistically uniform in the streamwise direction at any given time. This assumption is approached for small streamwise displacements in actual jets. The temporal configuration is commonly used in direct numerical simulation (DNS) where computational domain sizes are limited [17]. In DNS, there is a fixed streamwise expanse and the flow is periodic in the streamwise and spanwise directions so that there is a single direction of mean shear. The ODT line is oriented along this direction of mean shear.

Here, we consider a gaseous reacting jet in which the jet fluid consists of fuel, and the surrounding fluid is oxidizer (e.g., a combustion jet). Figure 4 shows the configuration of the temporal jet. The image is a DNS of an ethylene jet flame, with the orientation of the ODT line as shown. In this flow, three momentum components are transported along with chemical species and enthalpy describing the reacting flow. This configuration illustrates a reacting flow in which heat release causes flow dilatation through variations in the density. This dilatation will result in expansion of grid cells according to the Lagrangian evolution equations described below. In addition, thermodynamic and transport properties such as heat capacity and viscosity are temperature and composition dependent.

5.1.3 Conservation equations

The Lagrangian transport equations are derived beginning with the Reynolds transport theorem. Consider a system Ω containing a fixed/marked mass of fluid. This mass could be a mixture of species or a single component. The system is defined such that no mass (defining the system) crosses the system boundary Π. That is, the system boundary moves with the velocity of the mass defining the system. The Reynolds transport theorem written in terms of an intensive variable (some quantity per unit mass) β is given by

$$\frac{\mathrm{d}}{\mathrm{d}t}\int\limits_{\Omega}\rho\beta \mathrm{d}V = \frac{\mathrm{d}}{\mathrm{d}t}\int\limits_{\hat{\Omega}}\rho\beta \mathrm{d}V + \int\limits_{\hat{\Pi}}\rho\beta\mathbf{v}_R\cdot\mathbf{n}\mathrm{d}A. \tag{2}$$

Here, Ω denotes the Lagrangian system (with boundary Π), and $\hat{\Omega}$ a moving Eulerian control volume chosen to coincide with Ω at time t (and having boundary $\hat{\Pi}$). The velocity $\mathbf{v}_R$ is the relative velocity between the system boundary and the control volume boundary $\mathbf{v}_R = \mathbf{v}_\Pi - \mathbf{v}_{\hat{\Pi}}$. The control volume boundary velocity is taken, in all cases, to be the mass average velocity.

In the following sections, equations are presented for individual control volumes on the computational grid with quantities evaluated at the cell center. Flux terms and other quantities evaluated on cell faces are denoted with subscripts w and e to denote the left and right cell faces, respectively. Spatial derivatives appearing in heat, mass, and momentum flux terms are evaluated at cell faces using (nominally) second-order central differences so that, for cell i, $(\mathrm{d}\phi/\mathrm{d}x)_{i,e} = (\phi_{i+1}-\phi_i)/\frac{1}{2}(\Delta x_{i+1}+\Delta x_i)$ for some variable ϕ.

5.1.4 Continuity equation

Let $\beta = 1$ in Eq. (2), so that the system encloses the mixture mass and the system boundary moves with the mass average velocity so that $\mathbf{v}_R = 0$. Since there is no mass source term, Eq. (2) becomes

$$\frac{\mathrm{d}}{\mathrm{d}t}\int\limits_{\hat{\Omega}}\rho \mathrm{d}V = 0, \tag{3}$$

or, for uniform properties inside control volumes, and in 1D

$$\frac{\mathrm{d}}{\mathrm{d}t}(\rho\Delta x) = 0, \quad \Rightarrow \quad \rho\Delta x = C. \tag{4}$$

5.1.5 Species equation

For a diffusing species, take $\beta = Y_\alpha$. The system boundary moves with the velocity of the species, and the control volume boundary moves with the mass average velocity. Therefore, $\mathbf{v}_R = \mathbf{v}_\alpha - \mathbf{v}$ in Eq. (2). Also $\mathbf{v}_\alpha = \mathbf{v} + \mathbf{v}_\alpha^D$, where $\mathbf{v}_\alpha^D$ is the species diffusion velocity. The Lagrangian conservation law for species α is $\frac{\mathrm{d}}{\mathrm{d}t}\int_\Omega \rho Y_\alpha \mathrm{d}V = \int_\Omega \omega_\alpha \mathrm{d}V$, where ω_α is the species reaction rate. Substitution in Eq. (2), assuming uniform properties in 1D control volumes, using constant $\rho\Delta x$, and rearranging gives

$$\frac{\mathrm{d}Y_\alpha}{\mathrm{d}t} = -\frac{1}{\rho\Delta x}(j_{\alpha,e} - j_{\alpha,w}) + \frac{\omega_\alpha}{\rho}, \tag{5}$$

where, $\mathbf{j}_\alpha = \rho Y_\alpha \mathbf{v}_\alpha^D$ and subscripts e, and w denote east and west faces of control volumes. The diffusion flux model used for species α is a form of Fick's law:

$$j_\alpha = -\frac{\rho Y_\alpha D_\alpha}{X_\alpha}\frac{\mathrm{d}X_\alpha}{\mathrm{d}x} = -\rho D_\alpha\frac{\mathrm{d}Y_\alpha}{\mathrm{d}x} - \frac{\rho D_\alpha Y_\alpha}{M}\frac{\mathrm{d}M}{\mathrm{d}x}, \tag{6}$$

where M is the mean molecular weight, D_α is the species diffusion coefficient, and X_α is the mole fraction of species α.

5.1.6 Momentum equations

Here, take $\beta = \mathbf{v}$, and the system and control volume velocities are the same so $\mathbf{v}_R = 0$. Equation (2) becomes

$$\frac{\mathrm{d}}{\mathrm{d}t}\int\limits_{\Omega(t)} \rho\mathbf{v}\mathrm{d}V = \frac{\mathrm{d}}{\mathrm{d}t}\int\limits_{\hat{\Omega}(t)} \rho\mathbf{v}\mathrm{d}V. \tag{7}$$

The Lagrangian conservation law is $\frac{\mathrm{d}}{\mathrm{d}t}\int_{\Omega}\rho\mathbf{v}\mathrm{d}V = \int_{\Pi}\mathbf{F}_{\text{ext}}\mathrm{d}A = -\int_{\Pi}(P\boldsymbol{\delta}+\boldsymbol{\tau})\cdot\mathbf{n}\mathrm{d}A$. Making this substitution and integrating over the control volume as before gives:

u-Momentum:

$$\frac{\mathrm{d}u}{\mathrm{d}t} = -\frac{1}{\rho\Delta x}(\tau_{xx,e} - \tau_{xx,w}), \tag{8}$$

(neglecting pressure gradients along the line).

v-Momentum:

$$\frac{\mathrm{d}v}{\mathrm{d}t} = -\frac{1}{\rho\Delta x}(\tau_{yx,e} - \tau_{yx,w}) - \frac{1}{\rho}\frac{\mathrm{d}P}{\mathrm{d}y}, \tag{9}$$

(where the last term is a specified momentum source, here specializing to planar channel flow).

w-Momentum:

$$\frac{\mathrm{d}w}{\mathrm{d}t} = -\frac{1}{\rho\Delta x}(\tau_{zx,e} - \tau_{zx,w}), \tag{10}$$

(neglecting pressure gradients in the z-direction).

As written here, x is the line direction with the main velocity component (driving the eddies) being v; y is the cross-line direction; and z is a spanwise direction. In a channel flow, x would span the channel, y would be in the mean streamwise direction, and z would be the infinite spanwise direction. In the momentum equations, we neglect pressure gradients in the line-wise and span-wise directions.

The stress tensor is modeled as

$$\tau_{xx} = -\mu\frac{\mathrm{d}u}{\mathrm{d}x}, \qquad \tau_{yx} = -\mu\frac{\mathrm{d}v}{\mathrm{d}x}, \qquad \tau_{zx} = -\mu\frac{\mathrm{d}w}{\mathrm{d}x}. \tag{11}$$

5.1.7 Energy equation

The remainder of this section is specialized to combustion applications. To derive the energy equation, take $\beta = e$ in Eq. (2), where e is the internal energy per unit mass. The system contains the mixture mass so the system and control volume have the same velocities and $\mathbf{v}_R = 0$. The Lagrangian conservation law is

$$\frac{\mathrm{d}}{\mathrm{d}t}\int\limits_{\Omega}\rho e\mathrm{d}V = \dot{Q} + \dot{W} = -\int\limits_{\Pi}\mathbf{q}\cdot\mathbf{n}\mathrm{d}A - \int\limits_{\Pi}\mathbf{F}\cdot\mathbf{v}_{sys}\mathrm{d}A, \tag{12}$$

where $\mathbf{F}$ is the force per unit area acting on surface Π, and $\mathbf{q}$ is the heat flux vector. Considering only pressure work, and integrating over the 1D control volume yields

$$\frac{\mathrm{d}e}{\mathrm{d}t} = -\frac{1}{\rho\Delta x}(q_e - q_w) - \frac{P}{\rho\Delta x}(U_e - U_w), \tag{13}$$

where U denotes a dilatational velocity, and P is again assumed uniform on the line. Now insert $e = h - P/\rho$ and multiply through by $\rho\Delta x$:

$$\rho\Delta x\frac{\mathrm{d}h}{\mathrm{d}t} = \frac{\mathrm{d}(P\Delta x)}{\mathrm{d}t} - (q_e - q_w) - P(U_e - U_w) \tag{14}$$

$$= -(q_e - q_w) + \Delta x\frac{\mathrm{d}P}{\mathrm{d}t} + P\frac{\mathrm{d}\Delta x}{\mathrm{d}t} - P(U_e - U_w). \tag{15}$$

The last two terms in the second equation cancel, leaving

$$\frac{\mathrm{d}h}{\mathrm{d}t} = -\frac{1}{\rho\Delta x}(q_e - q_w) + \frac{1}{\rho}\frac{\mathrm{d}P}{\mathrm{d}t}. \tag{16}$$

The heat flux vector includes thermal conduction and species mass flux terms:

$$\mathbf{q} = -\lambda\frac{\mathrm{d}T}{\mathrm{d}x} + \sum_\alpha h_\alpha \mathbf{j}_\alpha. \tag{17}$$

5.1.8 Pressure equation

Pressure is assumed uniform on the grid, but may vary with time. This will be true for constant volume domain configurations (or with volume a specified function of time), along with periodic configurations, whereas outflow configurations consist of flow at constant pressure. The $\frac{\mathrm{d}P}{\mathrm{d}t}$ term in the energy equation is unknown and must be computed. This term is evaluated from the equation of state, following [3,20]. Start with

$$P = \frac{\rho RT}{M} = \rho RT\sum_\alpha \frac{Y_\alpha}{M_\alpha}. \tag{18}$$

Take the material derivative of this equation to obtain

$$\frac{\mathrm{D}P}{\mathrm{D}t} = \frac{\mathrm{d}P}{\mathrm{d}t} = \frac{RT}{M}\frac{\mathrm{D}\rho}{\mathrm{D}t} + \frac{\rho R}{M}\frac{\mathrm{D}T}{\mathrm{D}t} + \rho RT\sum_\alpha \frac{1}{M_\alpha}\frac{\mathrm{D}Y_\alpha}{\mathrm{D}t}. \tag{19}$$

The material derivatives on the right hand side of this equation are evaluated using the transport equations for density, species mass fractions, and temperature. For mass and species, these transport equations are

$$\frac{\mathrm{D}\rho}{\mathrm{D}t} = -\rho\nabla\cdot\mathbf{v}, \tag{20}$$

$$\frac{\mathrm{D}Y_\alpha}{\mathrm{D}t} = \frac{-\nabla\cdot\mathbf{j}_\alpha}{\rho} + \frac{\omega_\alpha}{\rho}. \tag{21}$$

For temperature, use $h = h(T, Y_\alpha)$ to obtain

$$\mathrm{d}h = \frac{\partial h}{\partial T}\mathrm{d}T + \sum_i \frac{\partial h}{\partial Y_\alpha}\mathrm{d}Y_\alpha = c_p\mathrm{d}T + \sum_\alpha h_\alpha \mathrm{d}Y_\alpha, \tag{22}$$

which yields

$$\frac{\mathrm{D}h}{\mathrm{D}t} = c_p\frac{\mathrm{D}T}{\mathrm{D}t} + \sum_\alpha h_\alpha\frac{\mathrm{D}Y_\alpha}{\mathrm{D}t}. \tag{23}$$

Solving For $\mathrm{D}T/\mathrm{D}t$ gives

$$\frac{\mathrm{D}T}{\mathrm{D}t} = \frac{1}{c_p}\frac{\mathrm{D}h}{\mathrm{D}t} - \frac{1}{c_p}\sum_\alpha h_\alpha\frac{\mathrm{D}Y_\alpha}{\mathrm{D}t}, \tag{24}$$

$$= -\frac{\nabla\cdot\mathbf{q}}{\rho c_p} + \frac{1}{\rho c_p}\frac{\mathrm{d}P}{\mathrm{d}t} + \frac{1}{\rho c_p}\sum_\alpha h_\alpha\nabla\cdot\mathbf{j}_\alpha - \frac{\omega_\alpha}{\rho c_p} \tag{25}$$

Now Eq. (19) becomes, upon inserting Eqs. (20, 21, 25) for $\mathrm{D}\rho/\mathrm{D}t$, $\mathrm{D}Y_\alpha/\mathrm{D}t$, and $\mathrm{D}T/\mathrm{D}t$, respectively, and solving for $\mathrm{d}P/\mathrm{d}t$

$$\frac{\mathrm{d}P}{\mathrm{d}t} = -\gamma P\nabla\cdot\mathbf{v} + \gamma P\mathcal{U}, \tag{26}$$

where Eq. (18) is used, along with $\gamma = c_p/c_v = c_p/(c_p - R)$. Here, $\mathcal{U}$ is given by

$$\mathcal{U} = \frac{1}{\rho c_p T}\left(-\nabla \cdot \mathbf{q} + \sum_\alpha h_\alpha(\nabla \cdot \mathbf{j}_\alpha - \omega_\alpha)\right) - \frac{M}{\rho}\sum_\alpha \frac{1}{M_\alpha}(\nabla \cdot \mathbf{j}_\alpha - \omega_\alpha). \tag{27}$$

In this equation, $\rho c_p T = MP\gamma/(\gamma - 1)$ may be used. Note that the form of this equation is equivalent to, but different than that reported in [20]. Equation (26) can be rearranged to give the dilatation of the fluid elements:

$$\nabla \cdot \mathbf{v} = -\frac{1}{\gamma P}\frac{\mathrm{d}P}{\mathrm{d}t} + \mathcal{U}. \tag{28}$$

This equation is integrated over control volumes individually to give the difference between cell face velocities for a given control volume:

$$\begin{aligned} U_e - U_w = &-\frac{\Delta x}{\gamma P}\frac{\mathrm{d}P}{\mathrm{d}t} + \frac{1}{\rho c_p T}\left(-(q_e - q_w) + \sum_\alpha h_\alpha(j_{\alpha,e} - j_{\alpha,w} - \omega_\alpha \Delta x)\right) \\ &-\frac{M}{\rho}\sum_\alpha \frac{1}{M_\alpha}(j_{\alpha,e} - j_{\alpha,w} - \omega_\alpha \Delta x). \end{aligned} \tag{29}$$

Then, $\frac{\mathrm{d}P}{\mathrm{d}t}$ is computed by integrating this equation over the domain and noting the uniform pressure:

$$U_{x=L} - U_{x=0} = -\frac{1}{P}\frac{\mathrm{d}P}{\mathrm{d}t}\int \frac{1}{\gamma}\mathrm{d}x + \int \mathcal{U}\mathrm{d}x, \tag{30}$$

where $U_{x=0}$, $U_{x=L}$ are the domain boundary velocities (usually zero). The result for $\frac{\mathrm{d}P}{\mathrm{d}t}$ is given by

$$\frac{\mathrm{d}P}{\mathrm{d}t} = \frac{\int \mathcal{U}\mathrm{d}x - (U_{x=L} - U_{x=0})}{\frac{1}{P}\int \frac{1}{\gamma}\mathrm{d}x}. \tag{31}$$

The integrals in this equation are evaluated on the 1D domain with uniform cell profiles, as above.

5.1.9 Solution procedure

The equation system represents a coupled set of ordinary differential equations that are solved explicitly in time using a Runge–Kutta method. These Eqs. (8–10) are for the u, v, and w momentum components, and (5), and (16) for species and enthalpy, respectively (if needed). Consider the first-order Euler method for discussion. The following solution procedure is used for a single time-step advancement from t_n to t_{n+1}:

1. Compute mass, heat, and momentum fluxes q, j, and τ at cell faces, along with reaction source terms for cells at time t_n.
2. Compute $\mathrm{d}P/\mathrm{d}t$ for use in the energy equation, if needed.
3. Advance the species Eq. (5), the u, v, w momentum equations (8, 9, 10), and the energy equation (16) to obtain Y_α, u, v, w, and h at t_{n+1}.
4. Advance the pressure using $\mathrm{d}P/\mathrm{d}t$, if needed.
5. Solve relations $M = M(Y_\alpha)$, and $h = h(T, Y_\alpha)$ for M and T, respectively, at t_{n+1}.
6. Solve the ideal gas law $\rho = \frac{MP}{RT}$ for ρ at t_{n+1}.
7. Solve $(\rho\Delta x)_n = (\rho\Delta x)_{n+1}$ for Δx at t_{n+1}, and modify the grid spacings.

Note that the mesh size Δx is a known function of the density and the initial condition (or any previous grid and density combination). Time integration is performed explicitly using either the first-order Euler method, or a second-order trapezoid method (sometimes called the modified Euler method [9]), both of which are in the class of Runge–Kutta methods [9]. The second-order method uses an Euler predictor to t_{n+1}, then steps using the average rate at the beginning of the step and the end of the step. That is, for $\mathrm{d}\phi/\mathrm{d}t = f(\phi)$ for some scalar ϕ,

$$\hat{\phi}_{n+1} = \phi_n + \Delta t f(\phi), \tag{32}$$

$$\phi_{n+1} = \phi_n + \frac{\Delta t}{2}(f(\phi_n) + f(\hat{\phi}_{n+1})). \tag{33}$$

5.1.10 Implicit chemistry

Explicit solutions with detailed chemical mechanisms can be prohibitively expensive due to small time steps required for stiff chemistry with fast reaction rates. A fully implicit solution would solve this problem, but would be very costly in that the whole domain would be coupled. An alternative that maintains explicit solution at the diffusion time scale, but removes stiff chemical time scales, is applied. In explicit, Runge–Kutta type methods, when computing values at t_{n+1}, all properties are assumed constant at values at t_n over the time step Δt. During the explicit advancement, the stiffness in the chemical source terms is mitigated (as an option) by modifying the reaction source appearing in the species equation as follows. First, the species and enthalpy equations for each cell are implicitly integrated over Δt independent of all other cells. The cells are normally coupled through the flux terms and these terms are retained in the implicit integration, but are assumed constant. (Note that these are assumed constant anyway over the time step Δt in an explicit method.) The integration results in mass fractions at the end of the implicit integration $\hat{Y}_{\alpha,n+1}$. The modified reaction source is taken as its mean over the implicit step, computed by

$$\left(\frac{\omega_i}{\rho}\right)_{\text{mean}} = \frac{\hat{Y}_{\alpha,n+1} - Y_{\alpha,n}}{\Delta t} + \left(\frac{1}{\rho \Delta x}(j_{\alpha,e} - j_{\alpha,w})\right)_n . \tag{34}$$

(Refer to the species equation Eq. (5).) The implicit integration is performed with CVODE [2]. In summary, the explicit advancement is done as described above, but with the reaction source term in the species equation replaced by its mean rate over the step, which is computed at any time with Eq. (34). In the second-order advancement, Eq. (34) is computed twice, once at the beginning of the step using fluxes evaluated at the beginning of the step, and again using fluxes evaluated at the end of the step, cf. Eq. (32). The integration order of this approach has been verified numerically to be the same as that of the low (first or second) order explicit advancement when a higher order implicit integration of the chemistry is performed.

Normally, the equations are advanced using the first-order method. While the second-order method is implemented, it is not very efficient, since the higher order integration is performed twice per step. A more efficient approach would be to use a second-order Strang splitting [27] in which one integrates diffusion without reaction for a half step, then integrates the reaction source without diffusion over the whole step (beginning with the solution at the half step), then integrates diffusion without reaction over another half step (beginning with the solution at the end of the reaction step).

5.2 Spatial advancement

The spatial formulation of ODT allows simulation of flows that are statistically 2D. The time dimension is replaced by evolution in a direction spatially orthogonal to the ODT line, obtained as the solution to a parabolic equation system. The spatial formulation amounts to solution of boundary layer-type equations. Jets, wakes, mixing layers, and plumes may all be represented using the boundary layer approximation. The primary assumption is that the streamwise velocity component dominates over other components, and that gradients are strongest in lateral directions with negligible diffusion in the streamwise direction. The 2D flow field is assumed steady in each flow realization, but with the addition of eddy events that perturb the flow field differently during each flow realization. Multiple flow realizations are conducted to obtain statistics. The randomness of eddy events causes the ensemble of realizations to have the statistical attributes of unsteady flow, though each realization obeys the governing equations of steady flow.

The formulation here is similar to that reported in [1], but is Lagrangian in the line direction. Because the flow is steady, the second term (the unsteady term on the right-hand side) in Eq. (2) is zero. That equation is then rewritten as

$$\left(\frac{\mathrm{d}}{\mathrm{d}t}\int_{\Omega} \rho\beta \mathrm{d}V\right) = \int_{\hat{\Pi}} \rho\beta \mathbf{v}_R \cdot \mathbf{n} \mathrm{d}A = \int_y \int_x \left(\frac{\partial \rho\beta v_{R,x}}{\partial x} + \frac{\partial \rho\beta v_{R,y}}{\partial y}\right) \mathrm{d}x\mathrm{d}y, \tag{35}$$

where the divergence theorem is applied to the second term. The first term of this equation is the evolution of the Lagrangian system, for which the Lagrangian conservation laws are inserted. The time derivative appearing in the equation reflects the rate of change of the property of the system being tracked and is consistent with the stationary nature of the flow. The derivative of this equation with respect to the evolution direction y is taken:

$$\frac{\mathrm{d}}{\mathrm{d}y}\left(\frac{\mathrm{d}}{\mathrm{d}t}\int\limits_{\Omega}\rho\beta\mathrm{d}V\right)=\int\limits_{x}\left(\frac{\partial\rho\beta v_{R,x}}{\partial x}+\frac{\partial\rho\beta v_{R,y}}{\partial y}\right)\mathrm{d}x \tag{36}$$

$$=(\rho\beta v_{R,x})_e-(\rho\beta v_{R,x})_w+\frac{\mathrm{d}}{\mathrm{d}y}(\rho\beta v_{R,y}\Delta x), \tag{37}$$

so that the result is integrated over the control volume in the line direction x, but remains differential in y.

5.2.1 Continuity, species, momentum, and energy equations

The conservation law for mass follows from Eq. (37), where mass has no source term, and $v_{R,x}=0$. This gives

$$\rho v\Delta x=C, \tag{38}$$

where C is a constant. For the spatial formulation, instead of mass conservation in cells, we have y-mass-flux conservation.

The Lagrangian conservation laws for species, momentum, and energy are obtained using Eq. (37) as they were obtained for the temporal formulation using Eq. (2). As in Eq. 38, it is the fluxes of these quantities that are spatially advanced. The resulting equation set is essentially the same as in a reported spatial ODT formulation [23]. The equations for species, momentum, and energy are very similar to the temporal equations in Sect. 5.1, but $\mathrm{d}/\mathrm{d}y$ replaces $\mathrm{d}/\mathrm{d}t$ and the rates on the right hand side are divided by v. The Lagrangian formulation accounts for dilatation along the ODT line associated with density change or with dilatations orthogonal to the line (which are linked by continuity to line advancement) by displacing and resizing mesh cells as dictated by the continuity equations given above.

As the ODT line advances spatially, regions of low velocity in the advancement direction have implied correspondingly large residence times, consistent with what occurs physically in steady spatially advancing flows. The present spatial formulation is physically more realistic than previous approaches that have interpreted temporal advancement as spatial advancement through a simple time-space transformation using a mean velocity of motion of the ODT line in the advancement direction, which does not account for the implied spatially varying residence time along the ODT line.

To avoid infinite or negative implied residence time, the ODT profile of velocity in the advancement direction must be positive everywhere on the ODT domain for spatial flows. For wall-bounded flows, the spatial step increment is limited by the resolution in the vicinity of the wall, both because cells are often smaller there to capture flow gradients at the wall, and also because the velocity approaches zero at the wall, implying that small spatial increments correspond to large time increments.

It is noteworthy that there is a class of constant-density temporal flows whose ODT representation involves dilatational flow along the ODT domain, namely, planar-symmetric and axisymmetric stagnation flows. These flows are generated by planar or round jets impinging on a flat plate or by opposed jets. A geophysical example is subsidence in the planetary boundary layer.

The common feature of these flows that causes ODT to be applicable is that some properties of these flows are laterally homogeneous in some volume containing the center-line or center-plane, so the statistics of these properties vary only in the streamwise direction. It is common to model laminar stagnation flow in 1D (including exactly solvable cases) [24]. Supplementing such a formulation with eddy events is a rough prescription for ODT simulation of the turbulent regime. In this instance, ODT is not a closed conservative system in 1D. The in-line velocity U, as in Eq. (29), is now a compressive flow, reflecting the net outward flow in the directions not represented in ODT.

6 Demonstrations and discussion

Three demonstration cases are presented as applications of ODT. These cases consist of a temporally evolving plane channel flow, a temporally evolving plane reacting jet, and a spatially evolving flow buoyantly driven by

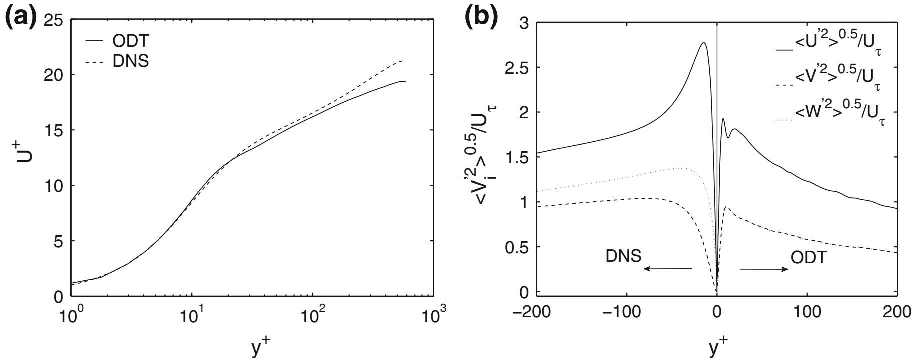

Fig. 5 ODT and DNS simulations of plane channel flow; **a** mean streamwise velocity; **b** root mean square fluctuations of velocity components for DNS (*left half*), ODT (*right half*)

an isothermal heated wall. A brief outline of the cases and key results are presented, followed by a discussion of these cases in the context of the mesh adaption and Lagrangian formulation.

The channel flow configuration was introduced in Sect. 5.1.1. Results are presented and compared to DNS at a Reynolds number of $Re_\tau = 590$. The DNS is from Moser et al. [19]. The ODT parameters used in the simulation (and described in the "Appendix") are $C = 10$, $Z = 600$. Also, eddy sizes are limited to half the channel width. Figure 5 shows the mean streamwise velocity (a), and the root mean square (RMS) profiles of the three velocity components (b). The profiles are shown in standard wall units [22]. Such comparisons have been reported previously, including discussion of sensitivity to adjustable parameters in ODT [25]. Naturally, the reduction in cost of ODT versus the DNS is enormous (several orders of magnitude), though the DNS provides much more realistic turbulence structures. The DNS consists of 38 million grid cells (384 in each direction). The corresponding ODT requires 2.2 min to run for 875 characteristic flow times (domain length divided by the average streamwise velocity) on one 2.8 GHz Intel Xeon processor, requiring an average of 260 grid cells on the adaptive mesh. (Results are unchanged on a finer grid of 650 (average) grid cells.) There is good agreement between the ODT and DNS for the mean streamwise velocity, and ODT is able to capture the transition from the viscous inner layer, through the buffer layer to the log-layer. As the wall is approached, eddy length scales decrease, and the adaptive ODT grid optimizes the placement of grid points to resolve the sharp near-wall gradients. This is illustrated in previous images taken from the channel flow, for example, Fig. 2. The RMS profiles in plot (b) show DNS on the left and ODT on the right. The ODT v and w velocities (inline and spanwise) are equal in this ODT configuration. The RMS profiles are somewhat lower for ODT than for DNS, but are qualitatively similar in behavior, and of similar magnitude. Better RMS results are obtained when ODT is used as a near-wall closure for LES [25].

An interesting feature that arises in ODT is the double peak near the wall in the streamwise velocity fluctuation, shown in Fig. 5, plot (b) near the center. This double peak is not observed in the DNS. It has been previously reported, but not fully described [25]. This feature represents an artifact generated by triplet map at the wall. Away from the wall, eddies are random in their location. The wall is a boundary that eddies cannot cross. It selectively excludes eddies in a manner that causes a degree of alignment of near-wall eddies. The triplet map is structured so that the largest variation in a profile generally occurs at eddy interior locations that are fractions $\frac{1}{3}$ and $\frac{2}{3}$ of the eddy size. The double peak is consistent with these fractions. This is shown in Fig. 6 where the probability density function (PDF) of locations at the $\frac{1}{3}$ and $\frac{2}{3}$ points within eddies are shown for those eddies that are at least partially contained within $y^+ < 60$. The smallest eddy size is $L^+ = 21$, and the most probable eddy size is $L^+ = 36$. There is a clear alignment between the location of the peak of the PDF of $\frac{1}{3}$ and $\frac{2}{3}$ fractional locations and the peaks in the streamwise velocity fluctuation profile. These peaks also are consistent with $\frac{1}{3}$ and $\frac{2}{3}$ the most probable eddy size.

Results of a planar, temporally evolving reacting jet simulation are shown in Fig. 7. Here, an ethylene fuel core is surrounded by oxidizer, both preheated to 550 K. A flame is initialized taking the fuel and oxidizer mixture (which transitions smoothly from pure oxidizer to pure fuel) as products of complete combustion. The velocity is initialized such that the Reynolds number is approximately 5,000. This configuration is being studied in detail and compared to DNS results [17]. The ODT parameters used in the simulation (and described in the "Appendix") are $C = 10$, $Z = 200$, and $\beta = 0.9$. Figure 7 shows the temperature and velocity profiles.

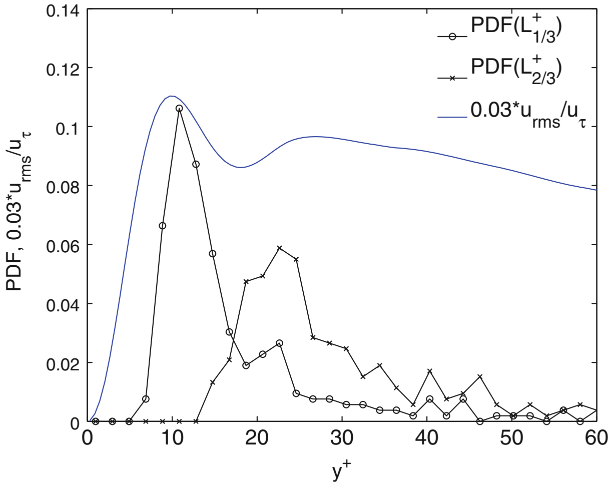

Fig. 6 PDF of $\frac{1}{3}$ and $\frac{2}{3}$ fractional locations within eddies and scaled u_{rms}

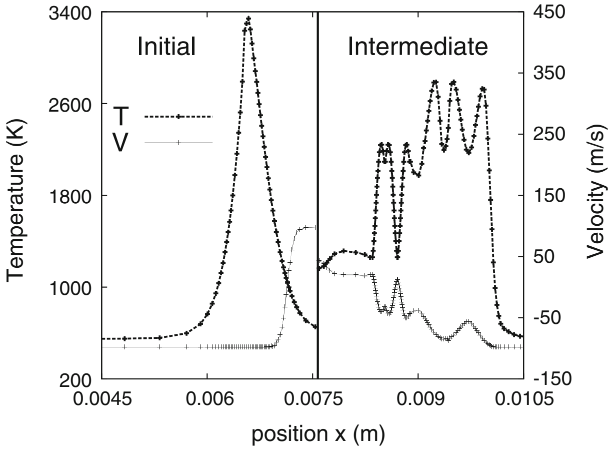

Fig. 7 Initial and intermediate instantaneous temperature and velocity profiles of a reacting temporal ethylene jet flame

The initial profile is shown on the left, and an intermediate profile is shown on the right. An adaptive grid is useful in reacting flow simulations since there may be many scalars whose length scales are very small. This may occur due to properties of the reaction zone or through varying property diffusivities. The figure illustrates the adaption of two scalars simultaneously. The initial variations in the temperature and velocity profiles do not strongly overlap, so that resolution of the temperature field results in over-resolved regions of the velocity field. Usually, adaption on temperature and velocity is sufficient to capture other intermediate species, but any of these can be included in the adaption as well, if desired.

To illustrate the spatial formulation of ODT, an isothermally heated wall is studied. The heated wall creates a vertical buoyant boundary layer flow with important applications in heat transfer. This case was previously studied by Shihn and DesJardin [26] using ODT. The case presented here is the first application of the formal spatial ODT formulation in [1,23] to a wall-bounded flow. This flow is challenging because the wall velocity is zero, so that the implied residence time diverges there. This singularity is avoided in the code since there is no grid cell at the wall. However, the required time-step size is small in this flow due to small cells near the wall, and also the low near-wall velocity divisor in the conservation equations. This motivates minimizing the number of cells in the simulation.

The simulation is of the experimental configuration of Tsuji and Nagano [30]. The ODT parameters used in the simulation (and described in the "Appendix") are $C = 3$, $Z = 900$, and $\beta = 1$. Figure 8a shows a spatial realization of the velocity field and a map of corresponding eddy sizes and locations. The velocity is initialized with a laminar boundary layer solution with a free stream velocity of 2 cm/s and a boundary layer thickness of 5 cm. The wall temperature here is 333 K, with surrounding air at 289 K. The upward velocity

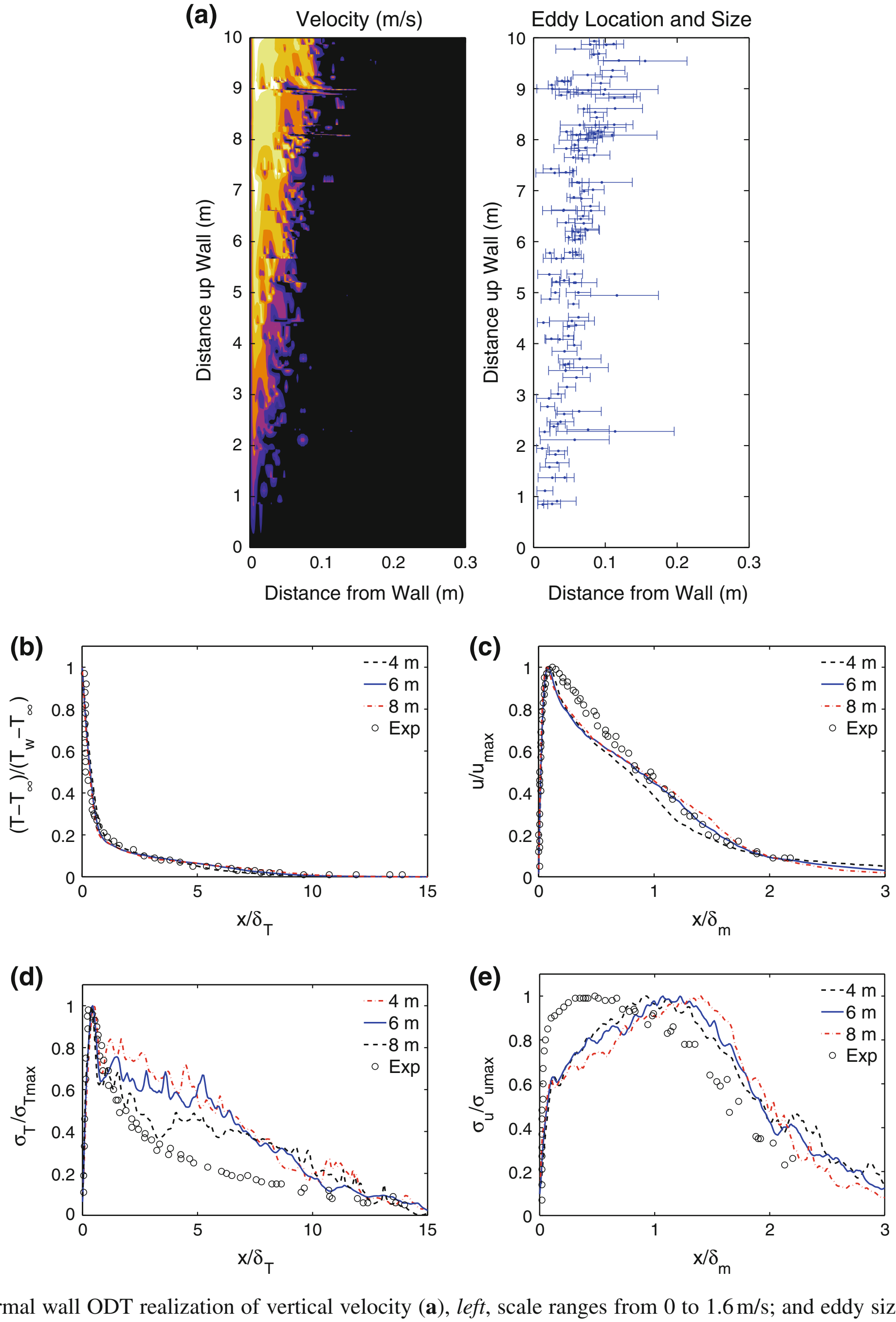

Fig. 8 Isothermal wall ODT realization of vertical velocity (**a**), *left*, scale ranges from 0 to 1.6 m/s; and eddy size and location map, *right*. Plots **b** and **c** show mean temperature and velocity profiles, respectively; plots **d** and **e** are the respective root mean square fluctuations

is zero at the wall, rises to a peak, then decays back to the zero ambient velocity with increasing distance from the wall. Eddy events tend to spread the flow, transferring heat from the wall to the air, and transferring buoyancy-generated momentum to the wall and the free stream. Conversely, as the air is accelerated upward, the conservation of mass flux results in air drawn inward and upward. The Lagrangian implementation of the inward motion on the ODT line results in contraction of the affected mesh cells during the spatial advancement. If left unchecked, this contraction could result in very small cells, indicating a role of mesh-adaption stemming from the kinematics of spatial advancement. Also shown in the figure is the sizes and locations of eddy events for a particular realization. Eddy events occur instantaneously and perturb the otherwise steady flow field. Many realizations are run, each with a different distribution of random eddies, to gather flow statistics.

Plots (b) and (c) in Fig. 8 show the mean temperature and velocity profiles normalized by the temperature difference between the wall and free stream and the max velocity, respectively, at three heights. The experimental wall height is 4 m. The abscissa is normalized by the thermal and momentum thickness. The agreement between the simulation and experiments is good. Profiles at three heights are shown in the figures and these profiles nearly overlap, highlighting the similarity solution. The root mean square fluctuations of temperature and velocity are shown in plots (d) and (e). The agreement is not as good here, but trends in the data are captured, and the magnitudes are very similar.

In Sect. 4, it was noted that mesh adaption causes some numerical dissipation. This dissipation is generally small compared to the physical dissipation in the problem and is minimized by selectively adapting only portions of the domain that need it. To quantify this, the kinetic energy dissipation associated with mesh adaption (which is unwanted) is compared to the kinetic energy dissipation due to the physical diffusion process (which is natural). The channel flow simulation was run with $N_{\text{dens}} = 30$ (a typical value) beginning with an instantaneous flow field at a statistically stationary state. The simulation was then run for 87 characteristic flow times without a pressure gradient so the turbulent flow decays somewhat. The total kinetic energy on the ODT line is computed before and after each mesh-adaption step, and the difference is taken. The sum of the absolute values of these differences is computed for the whole simulation (denoted KEA) and compared to the similar quantity around each diffusion operation (denoted KED), with diffusion operations entailing no mesh adaption. KEA is only 0.9 % of KED. With $N_{\text{dens}} = 100$, KEA is 0.2 % of KED. This indicates that the numerical dissipation of the mesh adaption is small compared to the physical dissipation and becomes smaller as the grid is refined.

The adaptive-mesh implementation reduces the computational cost of the simulation. There are several reasons for this; the most significant reason being the reduction in the number of grid cells compared to a uniform mesh with the same smallest cell size as an adaptive grid. Mesh adaption comes with a cost penalty through adaption and mesh management. In the channel flow simulation, profiling of the ODT code showed the direct mesh-adaption process required approximately 5 % of the overall simulation. Additional costs are incurred in mesh management of array structures in the code and there is room for improvement in the implementation. Even if the costs of mesh management were as high as 50 % of the overall simulation, the benefit from a reduction in the required number of grid cells would be more significant. In the temporal jet simulation with a one-step global mechanism consisting of five transported species (along with three velocity components and enthalpy), the diffusive advancement dominates all other processes. The diffusive advancement includes no adaption, cell insertions, etc. and so its cost (per cell) is similar in this code to diffusion costs on static grids.

In the channel flow simulation, run with $N_{\text{dens}} = 30$ and a minimum allowed cell size of 10 μm on a 2 m domain, the average number of grid cells was 260. The smallest cell size was 113 μm, and the most probable cell size was 575 μm. The ratio of the number of grid cells on a uniform mesh at the most probable cell size to the average number of cells in the adaptive grid is 13 (or 68 if the uniform mesh is taken at the smallest size generated by the mesh). In the temporal jet, the ratio with a uniform grid based on the most probable grid size is 8. The computational cost is roughly proportional to the number of grid points in a simulation, so that the ratio 13 (68) in the channel flow, or 8 in the temporal jet, may be considered a speedup factor. In the temporal jet, the ratio based on the most probable grid size was 8. This assumes a given fixed smallest cell size so that the time-step size is fixed, which is reasonable in comparing adaptive and uniform grids at the same small cell size. In the adaptive grid if the smallest required cell size increases, the allowed time-step size increases quadratically (based on a diffusion timescale $\Delta x_{\text{min}}^2/\nu$), further reducing computational costs.

Speedup factors will be less significant if static stretched meshes are used, and those can be viable alternatives. However, one must know a-priori where and how to stretch the mesh, or use some kind of dynamic adjustment procedure. Often, however, a simulation cannot be run efficiently on a static stretched mesh since the regions of interest (e.g., turbulent regions) may migrate, either intermittently, or as the flow evolves. The temporal jet is a case in point where the width of the jet increases in time, as does the required minimum cell size. A channel flow is statistically stationary, and a stretched mesh may do well, with a fine grid near the walls and a coarser grid in the outer (central) region. However, small eddies still occur in the central regions, and these would be under-resolved on a coarse mesh. Even within a given region of turbulence, dissipation structures tend to be thin and localized [29] and may benefit from local adaption.

The localization and variation of flow structures to be resolved is a key motivation for mesh adaption. In a recent application of the model to double diffusive flows [6], the formation of gravitationally stable interfaces causes sharp property jumps within small intervals whose locations are not known in advance and vary in time. While not quantified, large efficiency gains were found in tests of adaptive and uniform meshes.

Triplet maps require special attention on fixed grids. The triplet map cannot be implemented non-dissipatively on a fixed non-uniform mesh if momentum and scalars are conserved. For example, there would have to be mixing of properties mapped to a larger cell from multiple smaller cells. This highlights the point that the adaptive mesh allows a better triplet-map implementation than even on a uniform fixed mesh. Uniform meshes require discretization of the map size as well as location, and the discrete permutation only approximates the triplet map. Concerning this latter point, a size-six permutation induces only half as much dispersion (mean-square displacement) as in the continuum map of the same size. One can correct for this discrepancy by doubling the frequency of size-six maps, and analogously for larger maps, but this is not necessarily the only error resulting from the approximation. Thus, any fixed-mesh (uniform or stretched) implementation requires extra resolution so that the smallest maps are large enough relative to cell size to mitigate errors adequately. The adaptive-mesh map is subject to the error inherent in finite-volume discretization (piecewise constant vs. continuous functions), but not the additional errors that result from implementing the triplet map as a permutation, so overall, convergence to the continuum limit with increasing resolution is faster in principle, though this improved convergence has not yet been quantified.

7 Conclusions

In summary, it has been shown that implementation of ODT using a mesh that is both non-uniform and time varying has multiple benefits. In the spatial domain, it increases the computationally accessible scale range for a given number of mesh cells. In the time domain, it enables Lagrangian implementation of dilatation, thereby circumventing advective time-step restrictions.

Despite the simplifications inherent in 1D implementation, it has been shown that features unique to ODT impose atypical requirements and constraints on the mesh-adaption procedure. By construction, adaptive-mesh ODT generates ever-increasing mesh that must be compensated by ongoing culling of the mesh. New mesh cells are generated sporadically, so it is beneficial to adapt the mesh selectively in space and time to avoid adapting so intensively that unacceptably high numerical transport is induced.

A mesh-adaption procedure that fulfills these requirements has been described and demonstrated. It draws upon and improves upon a previously described approach [23]. Demonstrated and anticipated applications to combustion and to geophysical flows have been noted. In the geophysical realm, flows with sharp transitions between convective and stable layers, such as stratiform clouds, are promising targets, as are surface boundary layers, especially those in which it is important to resolve the distinct but coupled transport of momentum, heat, and species.

Acknowledgments This work was partially supported by the U.S. Department of Energy, Office of Basic Energy Sciences, Division of Chemical Sciences, Geosciences, and Biosciences. Sandia National Laboratories is a multi-program laboratory operated by Sandia Corporation, a Lockheed Martin Company, for the United States Department of Energy under contract DE-AC04-94-AL85000.

Appendix: Eddy sampling

The eddy sampling process is described here. As explained in Sect. 2, an eddy event consists of a triplet map applied to an interval $[x_0, x_0 + l]$ of the ODT domain followed by the addition of kernels to velocity profiles in this interval. Hence, an eddy is specified by a location x_0 and size l, denoted (x_0, l) for simplicity. Each possible eddy (x_0, l) has an associated timescale τ whose dependence on the flow state within the eddy interval is discussed below.

Given τ, an eddy rate per length squared is defined as

$$\lambda(x_0, l) = \frac{1}{\tau(x_0, l)l^2}, \tag{39}$$

and the total rate of all eddies is given by

$$\Lambda = \int_0^L \int_0^L \lambda(x_0, l)\mathrm{d}x_0\mathrm{d}l, \tag{40}$$

where the domain length L is the largest possible eddy size. The joint PDF of (x_0, l) is given by $P(x_0, l) = \lambda(x_0, l)/\Lambda$.

Eddy occurrences are deemed to be a Poisson process in time with rate Λ. In principle, eddy occurrences can be sampled based on Poisson statistics, and the values (x_0, l) for each can be sampled from the joint PDF $P(x_0, l)$. In practice, this is costly since $P(x_0, l)$ is constantly changing in a nontrival way as the flow evolves. After each change caused by an eddy event or diffusive advancement, one would have to reconstruct the two-dimensional $P(x_0, l)$, and sample from it by numerical inversion.

To avoid the unacceptable cost of this procedure, a thinning method [16] is used that is based on the rejection method [21]. This involves a guess $\tilde{P}(x_0, l)$ (preferably an accurate one) of $P(x_0, l)$. Candidate eddy occurrences are sampled based on Poisson statistics with rate $1/\Delta t_s$, where the sampling time Δt_s is chosen so that the sampling rate far exceeds Λ. For each candidate eddy, (x_0, l) are sampled from $\tilde{P}(x_0, l)$, and the candidate eddy is accepted with probability

$$P_a = \frac{\Delta t_s}{\tau l^2 \tilde{P}(x_0, l)}. \tag{41}$$

Δt_s is dynamically adjusted during the simulation to nudge the P_a values toward a target average acceptance probability $\overline{P_a}$ that is usually set to order 0.01 or less. Based on the physical modeling of τ (see below) and associated turbulence phenomenology, a reasonable initialization is $\Delta t_s = 0.1\overline{P_a} \cdot \overline{\Delta x}^2/(\nu n)$, where ν is kinematic viscosity, $\overline{\Delta x}$ is the average grid spacing, and n is the number of grid points. The quantity $\overline{\Delta x}^2/\nu$ is a diffusive time scale at the grid cell size, which is an approximate lower bound on an eddy timescale for the smallest, most frequent eddies. The factor $1/n$ reflects the proportionality of the total eddy rate to the domain size, and the factor of 0.1 is a conservative factor.

The chosen form of the PDF $\tilde{P}(x_0, l)$ is $\tilde{P}(x_0, l) = g(x_0) f(l)$. $g(x_0)$ is a uniform distribution over the possible x_0 values. $f(l)$ was modeled by S. Wunsch as described in [18]:

$$f(l) = \frac{2l_p}{l^2}\left[\frac{\exp(-2l_p/l)}{\exp(-2l_p/l_{\max}) - \exp(-2l_p/l_{\min})}\right], \tag{42}$$

where $l_{\min}$, $l_{\max}$, and l_p are user-specified minimum, maximum, and most probable eddy sizes, respectively. The accuracy of the guess $\tilde{P}(x_0, l)$ affects the efficiency of the eddy sampling process, but not the results of the simulation. That is, for a poor guess, eddies would have to be sampled at a higher rate to get the same number of accepted eddies as with a better guess of the PDF.

The eddy timescale τ, used to specify the eddy acceptance probability, is given by

$$\frac{1}{\tau} = C\sqrt{\frac{2}{\rho_0 l^3}(E_{\mathrm{kin}} - E_{\mathrm{pot}} - ZE_{\mathrm{vp}})}. \tag{43}$$

This equation is based on the scaling $E \sim \frac{1}{2}\rho_0 l^3/\tau^2$, where ρ_0 is a measure of the density in the eddy region for variable density flows, $\rho_0 = l^{-3}\int \rho K(x)^2 \mathrm{d}x$, and $K(x)$ is a kernel function discussed in Sect. 2 (also see [1,12]). The equation for $1/\tau$ has three terms: E_{kin}, E_{pot}, and E_{vp}. E_{kin} is a measure of the kinetic energy within the eddy interval and is specified as in [1] (also see below). E_{pot} is the potential-energy change induced by triplet mapping of the density profile if the ODT domain is vertically oriented and buoyancy effects are incorporated. This change is assumed to cause an equal-and-opposite change in kinetic energy, so in effect, $E_{\mathrm{kin}} - E_{\mathrm{pot}}$ represents the post-map kinetic energy.

E_{vp} is a viscous penalty term. It suppresses small eddies that are subject to strong viscous damping. If $ZE_{\mathrm{vp}} > E_{\mathrm{kin}} - E_{\mathrm{pot}}$, the eddy is suppressed. E_{vp} is modeled as $E_{\mathrm{vp}} = \frac{1}{2}\bar{\mu}^2/\bar{\rho} l$, where $\bar{\mu}$ and $\bar{\rho}$ are the average viscosity and density, respectively, within the eddy interval.

C and Z are ODT model parameters—the eddy rate parameter and the viscous penalty parameter, respectively, which are tuned for any given simulation. C scales turbulent transport but not turbulence intensity as measured by velocity fluctuations. Hence, it is roughly analogous to the coefficient of an eddy viscosity formula, with the crucial distinction that it tunes the advancement of a spatially and temporally resolved unsteady simulation rather than an ensemble-averaged state. Z can in principle be omitted (set to zero), but then the mesh discretization imposes an eddy-size cutoff implicitly. Thus, nonzero Z can be used to enforce mesh insensitivity of model implementation, although this can also be achieved at greater cost by refining the mesh until the unresolved eddies have negligible effect on computed results.

As the viscous penalty parameter is used to suppress small eddies, a large eddy suppression mechanism is required to prevent unphysically large eddies from occurring in open domains. These large eddies can have a strong impact on overall turbulent entrainment and mixing rates. Several large eddy suppression methods have been described including the scale reduction and median methods [1], and the elapsed time method [4,8]. The elapsed time method is given by the criterion $t > \beta\tau$ so eddies are only allowed if the elapsed simulation time is greater than $\beta\tau$, where β is an adjustable parameter. This method is used in the simulations presented in this paper.

The appearance of $K(x)$ (here termed a kernel, reflecting its wavelet-like role) in the definition of ρ_0 hints at the role of the kernels J and K in the sampling of eddies as well as in the enforcement of conservation laws. Specifically, E_{kin} is not taken to be the total kinetic energy within the eddy interval, but rather, is a measure of the portion of the kinetic energy attributable to velocity fluctuations at scale l. This reflects the scale locality of the turbulent cascade. Namely, motions at a given scale are driven by property fluctuations at roughly the same scale. (For example, a sinusoidal velocity variation with wavelength much less than l has little influence on the generation of a size-l motion.)

On this basis, the contribution of a given velocity component to E_{kin} is taken to be the maximum reduction of component kinetic energy that is achievable by adding $bJ + cK$ to that velocity component, with b and c varied subject to momentum conservation (which removes one degree of freedom). E_{kin} is thus an available (meaning extractable using kernels) kinetic energy, analogous to available potential energy in buoyant stratified flow.

To formalize this analogy, note that $-E_{\text{pot}}$ as defined above is the CAPE associated with a triplet map (see Sect. 2). E_{pot} can be expressed as $g\int(x'-x)\rho(x')\,\mathrm{d}x'$, where ρ is a mass per unit length in ODT and $x(x')$ is the location that is mapped to x' by the triplet map. Here, x' is the independent variable because $x(x')$ is single-valued but $x'(x)$ is triple-valued. The choices $K(x') = x' - x$ and $J = |K|$ are adopted because they align (somewhat) the mathematical representations of available kinetic and potential energy and because they are simple functions that serve the intended purpose. In particular, their use in determining E_{kin} admits only contributions from velocity variations over order-l spatial scales.

These choices are not unique, and energy-based modeling of τ is not mandatory. In fact, the original ODT formulation modeled τ using the integral of the velocity profile times a piecewise-constant function that is odd in $x_0 + \frac{l}{2}$ rather than additive kernels [10]. The performance of the two formulations is basically the same (e.g., compare [13] and [12]), but the energy-based formulation is more readily generalized within a conservative framework.

References

1. Ashurst, W.T., Kerstein, A.R.: One-dimensional turbulence: variable density formulation and application to mixing layers. Phys. Fluids **17-025107**, 1–26 (2005)
2. Cohen, S., Hindmarsh, A.: CVODE, a stiff/nonstiff ODE solver in C. Comput. Phys. **10**, 138–143 (1996). http://llnl.gov/casc/sundials/
3. Day, M.S., Bell, J.B.: Numerical simulation of laminar reacting flows with complex chemistry. Combust. Theory Model. **4**, 535–556 (2000)
4. Echekki, T., Kerstein, A.R., Dreeben, T.D.: One-dimensional turbulence simulation of turbulent jet diffusion flames: model formulation and illustrative applications. Combust. Flame **125**, 1083–1105 (2001)
5. Echekki, T., Kerstein, A.R., Sutherland, J.C. : The one-dimensional-turbulence model. In: Echekki, T., Mastorakos, E. (eds.) Turbulent Combustion Modeling: Advances, New Trends, and Perspectives, pp. 249–276. Springer, Heidelberg (2011)
6. Gonzalez-Juez, E., Kerstein, A.R., Lignell, D.O.: Fluxes across double-diffusive interfaces: a one-dimensional-turbulence study. J. Fluid Mech. **677**, 218–254 (2011)
7. Hack, J.J., Pedretti, J.A.: Assessment of solution uncertainties in single-column modeling frameworks. J. Clim. **13**, 352–365 (2000)
8. Hewson, J.C., Kerstein, A.R.: Stochastic simulation of transport and chemical kinetics in turbulent $CO/H_2/N_2$ flames. Combust. Theory Model. **5**, 669–697 (2001)
9. Hoffman, J.D.: Numerical Methods for Engineers and Scientists. CRC Press, New York (2001)

10. Kerstein, A.R.: One-dimensional turbulence: model formulation and application to homogeneous turbulence, shear flows, and buoyant stratified flows. J. Fluid Mech. **392**, 277–334 (1999)
11. Kerstein, A.R.: One-dimensional turbulence stochastic simulation of multi-scale dynamics. Lect. Notes Phys. **756**, 291–333 (2009)
12. Kerstein, A.R., Ashurst, W.T., Wunsch, S., Nilsen, V.: One-dimensional turbulence: vector formulation and application to free shear flows. J. Fluid Mech. **447**, 85–109 (2001)
13. Kerstein, A.R., Dreeben, T.D.: Prediction of turbulent free shear flow statistics using a simple stochastic model. Phys. Fluids **12**, 418–424 (2000)
14. Kerstein, A.R., Wunsch, S.: Simulation of a stably stratified atmospheric boundary layer using one-dimensional turbulence. Bound Lay. Meteorol. **118**, 325–356 (2006)
15. Krishnamoorthy, N.: Reaction Models and Reaction State Parameterization for Turbulent Nonpremixed Combustion. Ph.D. Thesis, The University of Utah (2008)
16. Lewis, P.A., Shedler, G.S.: Simulation of nonhomogeneous poisson processes by thinning. Naval Res. Logist. Q. **26**, 403–413 (1979)
17. Lignell, D.O., Chen, J.H., Schmutz, H.A.: Effects of Damköhler number on flame extinction and reignition in turbulent nonpremixed flames using DNS. Combust. Flame **158**, 949–963 (2011)
18. McDermott, R.J.: Toward One-dimensional Turbulence Subgrid Closure for Large-eddy Simulation. Ph.D. thesis, The University of Utah (2005)
19. Moser, R.D., Kim, J., Mansour, N.N.: Direct numerical simulation of turbulent channel flow up to Re_τ=590. Phys. Fluids **11**, 943–945 (1999). http://turbulence.ices.utexas.edu/MKM_1999.html
20. Oevermann, M., Schmidt, H., Kerstein, A.R.: Investigation of autoignition under thermal stratification using linear eddy modeling. Combust. Flame **155**, 370–379 (2008)
21. Papoulis, A., Pillai, S.U.: Probability, Random Variables, and Stochastic Processes, 4th edn. McGraw-Hill, New York (2002)
22. Pope, S.B.: Turbulent Flows. Cambridge University Press, New York (2000)
23. Ricks, A.J., Hewson, J.C., Kerstein, A.R., Gore, J.P., Tieszen, S.R., Ashurst, W.T.: A spatially developing one-dimensional turbulence (ODT) study of soot and enthalpy evolution in meter-scale buoyant turbulent flames. Combust. Sci. Technol. **182**, 60–101 (2010)
24. Schlichting, H., Gersten, K.: Boundary-Layer Theory, 8th edn. Springer, Heidelberg (2000)
25. Schmidt, R.C., Kerstein, A.R., Wunsch, S., Nilsen, V.: Near-wall LES closure based on one-dimensional turbulence modeling. J. Comput. Phys. **186**, 317–355 (2003)
26. Shihn, H., DesJardin, P.E.: Near-wall modeling of an isothermal vertical wall using one-dimensional turbulence. Int. J. Heat Mass Transf. **50**, 1314–1327 (2007)
27. Strang, G.: On the construction and comparison of difference schemes. SIAM J. Numer. Anal. **5**, 506–517 (1968)
28. Stull, R.B.: An Introduction to Boundary Layer Meteorology, 1st edn. Kluwer, Dordrecht (1988)
29. Su, L.K., Clemens, N.T.: The structure of fine-scale scalar mixing in gas-phase planar turbulent jets. J. Fluid Mech. **488**, 1–29 (2003)
30. Tsuji, N.: Velocity and temperature measurements in a natural convection boundary layer along a vertical flat plate. Exp. Therm. Fluid Sci. **2**, 208–215 (1989)